

Northerly surface winds over the eastern North Pacific Ocean in spring and summer

Stephen V. Taylor,^{1,2} Daniel R. Cayan,^{1,3} Nicholas E. Graham,^{1,2} and Konstantine P. Georgakakos^{1,2}

Received 18 September 2006; revised 5 August 2007; accepted 18 October 2007; published 24 January 2008.

[1] Persistent spring and summer northerly surface winds are the defining climatological feature of the western coast of North America, especially south of the Oregon coast. Northerly surface winds are important for upwelling and a vast array of other biological, oceanic, and atmospheric processes. Intermittence in northerly coastal surface wind is characterized and wind events are quantitatively defined using coastal buoy data south of Cape Mendocino on the northern California coast. The defined wind events are then used as a basis for composites in order to explain the spatial evolution of various atmospheric and oceanic processes. Wind events involve large-scale changes in the three-dimensional atmospheric circulation including the eastern North Pacific subtropical anticyclone and southeast trade winds. Composites of QSCAT satellite scatterometer wind estimates from 1999 to 2005 based on a single coastal buoy indicate that wind events typically last 72–96 h and result in anomalies in surface wind and Ekman pumping that extend over 1000 km from the west coast of North America. It may be useful to consider ocean circulation and dependent ecosystem dynamics and the distribution of temperature, moisture, and aerosols in the atmospheric boundary layer in the context of wind events defined herein.

Citation: Taylor, S. V., D. R. Cayan, N. E. Graham, and K. P. Georgakakos (2008), Northerly surface winds over the eastern North Pacific Ocean in spring and summer, *J. Geophys. Res.*, 113, D02110, doi:10.1029/2006JD008053.

1. Introduction

1.1. Background

[2] Persistent and relatively strong northerly surface wind offshore the U.S. West Coast in spring and summer arises from the sea level pressure (SLP) gradient between the eastern North Pacific high and relatively low pressure over the southwestern United States [Nelson, 1977; Halliwell and Allen, 1987]. Figure 1 shows the mean winds and SLP for April–August. The equatorward pressure gradient along the U.S. West Coast is the strongest and most persistent in North America [Brost *et al.*, 1982]. Subsidence associated with the high-pressure system helps to maintain and strengthen a temperature inversion and marine boundary layer in the lower troposphere. Coastal geometry combined with large-scale atmospheric circulation, oceanic upwelling of relatively cold water, thermal land heating, and marine boundary layer are parts of a coupled ocean-atmosphere-land system that includes relatively persistent and moderate equatorward surface wind [Seager *et al.*, 2003; Miyasaka and Nakamura, 2005]. This coupled system maintains mild summer temperatures and is

the dominant climatic feature of subtropical western continental coasts of the world [Lorenz, 1969; Mass *et al.*, 1986; Winant *et al.*, 1988; Parrish *et al.*, 2000].

[3] Baroclinicity from the horizontal temperature gradient between relatively cool ocean surface and warm land causes the inversion to slope downward toward the coast with enhanced wind speed adjacent to the coast [Neiburger *et al.*, 1961; Baynton *et al.*, 1965; Burk and Thompson, 1996]. Coastal terrain channels wind leading to further enhancement. However, modeling studies with flat terrain demonstrate the wind is mainly a product of large-scale circulation features and forcing [Burk and Thompson, 1996; Hoskins, 1996].

1.2. Motivation

[4] Wind along the U.S. West Coast has been the subject of numerous observational investigations because of its importance for biological and oceanic processes, prominence in the climate system, and threat to human activities. Previous studies have focused on fog and marine stratocumulus formation and dynamics [Fosberg and Schroeder, 1966; Klein *et al.*, 1995; Filonczuk *et al.*, 1995; Burk and Thompson, 1996; Rogers *et al.*, 1998; Koracin *et al.*, 2001; Thompson *et al.*, 2005], radar propagation [Haack and Burk, 2001] and radiative properties [Pincus *et al.*, 1997] of the marine boundary layer, air pollution [Dabberdt and Viezee, 1987], and ocean surface and subsurface currents and dynamics (including upwelling of cold, nutrient-rich subthermocline water) [Nelson, 1977; Huyer, 1983; Beardsley *et*

¹Scripps Institution of Oceanography, University of California, San Diego, La Jolla, California, USA.

²Also at Hydrologic Research Center, San Diego, California, USA.

³Also at U.S. Geological Survey, La Jolla, California, USA.

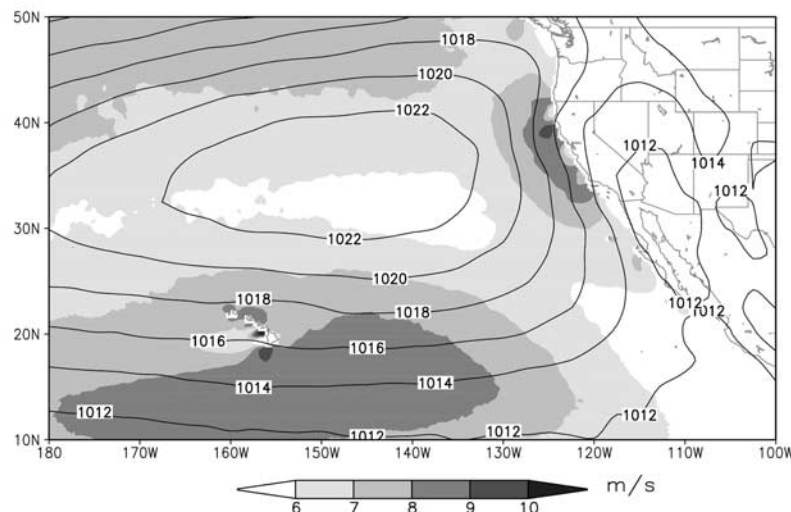


Figure 1. April–August climatological mean wind speed (from QSCAT satellite 2000–2005) with sea level pressure in mbar (from NCEP Reanalysis 1982–2005).

al., 1987; Miller *et al.*, 1999; Münchow, 2000]. In addition, spring and summer winds along the California coast produce wind waves and hazardous conditions [Lovegrove, 2003] affecting small craft, coastal and marine structures, commercial, recreational and certain naval operations. More recently, the prospects for offshore wind energy production have gained interest [Yen-Nakafuji, 2005].

[5] In the past, observations have been limited to climatologies and measurement campaigns of relatively short duration, relatively poor spatial coverage, or both. Information about the wind more than 30 km offshore is particularly lacking. Routine, fixed point measurements, observational campaigns, and previous satellite studies noted the event-like character of the wind but could not adequately address the spatial structure or evolution of wind events. Now, with more than 6 years of twice daily satellite scatterometer wind estimates at 25 km resolution, it is possible to examine surface wind variability in space and time with unprecedented detail.

[6] The temporal, and to some extent, spatial variability of winds along the California coast has been investigated in a number of studies using buoy, land station, and platform or similar fixed point measurements, aircraft flights, soundings and ship observations recorded during measurement campaigns lasting from a few days to 2 years [e.g., Neiburger *et al.*, 1961; Elliot and O'Brien, 1977; Caldwell and Stuart, 1986; Beardsley *et al.*, 1987; Dorman and Winant, 1995; Burk and Thompson, 1996; Rogers *et al.*, 1998; Dorman *et al.*, 1999; Edwards *et al.*, 2002].

[7] Understanding of the spatial scale of the high wind region along the coast is gleaned from nonsynoptic seasonal or monthly averages. Nelson [1977] and Bakun and Nelson [1991] used 100+ years of ship data averaged in $1^\circ \times 1^\circ$ grids to plot monthly mean wind stress. Winant and Dorman [1997] used 50 years of California Cooperative Oceanic Fisheries Investigation (CalCOFI) station observations to produce seasonal mean wind stress with about 65 km horizontal resolution. The CalCOFI sampling is irregular in time but seasonal averages are based on roughly one observation per station per season over 50 years.

[8] Buoy winds along the coast behave in a spatially coherent manner over broad scales of 1000 km or more [Halliwell and Allen, 1987]. Analysis of hourly wind data from buoys, platforms, and land stations near Point Conception [Caldwell and Stuart, 1986; Dorman and Winant, 2000] and Point Arena [Beardsley *et al.*, 1987] indicates that mean coastal conditions include moderate to gale-force northwesterly winds lasting days to weeks interrupted by brief periods (1–6 d) of calm or southerly wind. Enhanced northwesterly winds are characterized as lasting 1–2 d [Halliwell and Allen, 1987] up to 1 week [Huyer, 1983; Caldwell and Stuart, 1986; Beardsley *et al.*, 1987]. Beardsley *et al.* [1987] also describe northwest wind 7–15 m/s lasting up to 30 d. The discrepancy in the estimated duration of wind events may be attributed to relatively short analysis periods and the qualitative definitions of "enhanced" winds.

[9] Satellite wind estimates have also been used to average wind along the coast over 1–4 months. Dorman *et al.* [2000] show satellite derived mean winds for June–July 1996, while Edwards *et al.* [2002] show mean winds for June 1994 and June 1996. Both studies use SSM/I passive satellite wind estimates at $0.25^\circ \times 0.25^\circ$ resolution [Wentz, 1997]. Perlin *et al.* [2004] use Quikscat satellite scatterometer (active radar) wind estimates with 25 km resolution and depict mean winds for June–September 2000 and 2001. Note that passive satellite wind estimates are obtained via fundamentally different physics relative to active radar scatterometry used in the present study. Passive satellite wind estimates lack directional information and will have different error characteristics. Data and data accuracy will be covered in more detail in the next section.

[10] Coastal upwelling is extremely important for coastal biological productivity and it is relatively easy to study with short cruises, land based measurements, and moored instruments. As such, coastal upwelling has been extensively studied. The offshore region is less well examined for obvious reasons. Huyer [1983] indicates the importance of upwelling farther offshore. Recent research [Chelton *et al.*, 2004; Perlin *et al.*, 2004] demonstrates the offshore wind field is not smooth and strong winds are not confined to

Table 1. NDBC Buoy Wind Observations

Buoy 460##	Latitude, °N	Longitude, °W	Start Year	% Coverage
14	39.22	123.97	1981	88.3
59	37.98	130	1994	81.3
63	34.25	120.66	1982 ^a	77.5

^aData for buoy 23 prior to 1997 has been included in the buoy 63 record for this paper. Buoy 63 was established after 1997 at its current location, which is close to the former location of buoy 23 (prior to 1997). Buoy 23 was established at its current location, farther north, in 1997.

near-coast regions offshore of the U.S. West Coast. They find strong gradients in wind speed tied to sea surface temperature gradients hundreds of km offshore of the California and Oregon coasts.

[11] Features of the offshore Ekman pumping may be significant. *Hickey et al.* [2006] suggest the California Current system may be forced by remote wind stress in addition to local wind forcing. With the prospect of climate change and its effects on the California Current Ecosystem [Bakun, 1990; Synder et al., 2003; Grantham et al., 2004; Pierce et al., 2006], there is increased urgency in documenting and understanding offshore wind and Ekman pumping features.

[12] The motivation is in part fueled by new technology. Satellite scatterometer wind observations allow analysis of the spatial structure of winds with unprecedented detail. Data and Methods are presented below followed by Analyses which are broken into three main subsections including characterization of springtime northerly winds, a quantitative definition of wind events, and the evolution of wind events as seen in composites. The third subsection contains four parts, the final one discussing the curl of wind stress anomalies. Concluding remarks are found in section 5.

2. Data

2.1. Buoy Winds

[13] Buoy wind measurements are available from NOAA National Data Buoy Center, or NDBC (<http://www.ndbc.noaa.gov>). NDBC maintains an archive of about 75 moored buoys in the northeast Pacific Ocean with over 40 currently in operation. The historical record spans from late 1975 to present. Three buoys were chosen for analysis (Table 1 and Figure 2) on the basis of the duration and continuity of the record. Buoys where diurnal effects clearly dominate synoptic variability were not included (e.g., 46025), since diurnal effects are not a focus of this study.

[14] Wind speed is reported hourly on the basis of 8.5 min averages from anemometers located 5 m above sea level. Since the mid-1980s, R.M. Young Model 05103 anemometers have been used (NDBC website <http://www.ndbc.noaa.gov/improvements.shtml>). Wind speed and wind direction are scalar and vector averages, respectively. Some wind speed data from the 1980s employed vector averaging. Where applicable, these winds were slightly enhanced following *Gilhousen* [1987].

[15] NDBC wind accuracy for standard wind observations is listed as 1 m/s and 10° [Hamilton, 1980]. However, the accuracy may be better. *Gilhousen* [1987] performed extensive comparisons of winds from buoys located within approximately 100 km of each other. The standard deviation

of wind speed difference was 0.6 to 0.8 m/s for buoys separated by less than 5 km. Scatterplots of wind speed were linear and no bias was evident with wind speed magnitude. The calibration was stable with negligible drift over the lifetime of buoy deployment in several tests. The standard deviation of wind direction differences was 9 to 11°. *Gilhousen* [1987] also compared results from standard 8.5 min wind averages to 1 h averages. The differences were similar to those obtained between duplicate anemometers on the same platform (i.e., less than 1 m/s and 11°).

[16] For this study, standard meteorological buoy observations were scaled to 10 m from 5 m using power law scaling [Hsu et al., 1994, Figure 5] for near-neutral stability, despite evidence that surface stability conditions are, on average, slightly unstable [Koracin et al., 2001]. Air and sea surface temperature differences are generally within 2° in the study region and errors introduced in scaling are less than 10% in wind speed.

2.2. NCEP Global Reanalysis (R-1)

[17] Global Reanalysis fields of operational weather forecasts [Kalnay et al., 1996; Kistler et al., 2001] from the National Center of Environmental Prediction (NCEP) were obtained from <http://dss.ucar.edu/pub/reanalysis/>. Sea level



Figure 2. Geographical reference and buoy locations. Numbers mark approximate location of buoys from Table 1. Three prominent protrusions along the coast are Cape Mendocino, Point Conception, and Punta Eugenia. Buoy 14 is located at Point Arena, just south of Cape Mendocino. Buoy 63 is located near Point Conception. Buoy 59 is located relatively far offshore from the coast.

pressure, omega, U-wind, V-wind, surface temperature and geopotential height data are available at 6-hourly intervals with 2.5° latitude-longitude spacing from 1948 to the present. The NCEP reanalysis fields are a combination of historical data and a dynamically consistent atmospheric numerical weather prediction model, produced in much the same way that global analyses are produced today. Assimilation of raw atmospheric data, processing and interpolation occur under one, universally consistent scheme designed to eliminate perceived jumps in the climatic record associated with changes in data retrieval and assimilation techniques. The process begins with a first guess model 6-h forecast from the previous postprocess analysis combined and optimally interpolated with contemporaneous observations (e.g., rawinsonde, land surface station, ship reports, etc.). This new analysis updates the model before producing the next 6-h forecast and the cycle continues. The T62 global spectral forecast model includes 28 levels with 5 in the boundary layer. The model is nearly identical to the NCEP Medium Range Forecast (MRF) operational forecast system implemented in 1994. A description of the model is detailed by *National Meteorological Center Development Division Staff* [1988] and summarized by *Kanamitsu* [1989]. NCEP estimates the reliability of each variable based (“A” being the most reliable and “D” the least reliable). Level “A” variables are the most influenced by actual observations and are the most reliable. Observations directly affect the value of level “B” variables, though model dynamics exert some influence as well. SLP, U-wind, V-wind, temperature, and geopotential height as level “A” level products, while surface wind (U10, V10) and surface temperature are level “B” product. NCEP global Reanalysis fields have been used in well over a thousand publications in peer-review journals.

2.3. Satellite Scatterometer Winds

[18] Wind speed and direction estimates from the microwave radar scatterometer on board the QuikScat satellite [*Liu*, 2002; *Liu and Xie*, 2001] are available from 20 July 1999 to present. The satellite was launched in July 1999 and is operated by NASA. QuikScat (QSCAT) data are produced by Remote Sensing Systems and sponsored by the NASA Ocean Vector Winds Science Team. Data are available at <http://www.remss.com>.

[19] The polar orbiting satellite features a 1600 km swath with two passes, which collectively cover 90% of the globe at 25 km resolution each day. The daily spatial coverage and horizontal resolution are superior to any previous scatterometer missions [*Chelton et al.*, 2004] and offer a significant advantage over sparse in situ measurements from buoys, ships, or short-duration intensive observations programs.

[20] Previous publications detail scatterometer physics [*Naderi et al.*, 1991; *Liu*, 2002], QSCAT specifications [*Freilich et al.*, 1994], and instrument accuracy including comparisons with in situ observations [*Draper and Long*, 2002; *Ebuchi et al.*, 2002; *Chelton and Freilich*, 2005]. The RSS website above also contains more information. A brief overview relevant to this study is given below.

[21] The QSCAT scatterometer wind estimates are obtained via active microwave radar and are fundamentally different from passive microwave radiometry (e.g., SSM/I

instrument [*Wentz*, 1997; *Mears et al.*, 2001]). Microwave Ku-band (frequency near 14 GHz) pulses transmitted and received at the satellite backscatter from the sea surface. The backscatter signal from the rough sea surface is highly correlated with both wind speed and wind direction. Wind speed and direction are inferred from multiple backscatter cross-section signals with elliptical horizontal dimensions of 25 by 35 km obtained at systematically varying azimuths along the orbital track. Conversion to the equivalent 10-m wind speed assumes a neutrally stratified atmospheric boundary layer (following *Liu and Tang* [1996], with drag coefficient from *Large and Pond* [1982]) and interpolated onto a 0.25° grid.

[22] Overall accuracy in wind speed and wind direction is 1.5 m/s and 21° [*Chelton and Freilich*, 2005]. The accuracy is neither homogeneous nor isotropic across the swath. Accuracy varies by 0.1 m/s and 5° across the swath, independent of wind direction. Wind speed accuracy is 0.75 m/s for wind along the orbital track and 1.5 m/s for wind oriented across the track [*Chelton and Freilich*, 2005]. Comparisons with buoys [*Ebuchi et al.*, 2002; *Draper and Long*, 2002; *Bourassa et al.*, 2003] indicate a difference in standard deviation of 1.2 m/s and mean bias of 0.11 m/s relative to buoys for wind speeds between 2 and 18 m/s. For winds from 18 to 25 m/s the standard error increases to 10%. Buoy measurements of wind events studied in this paper rarely exceed 18 m/s and never reach 20 m/s.

[23] Further error may be attributed to the neutral stability assumption. *Chelton and Freilich* [2005] found the assumption leads to a mean bias of +0.2 m/s in QSCAT wind speed in the eastern North Pacific Ocean. The overestimate was found in other satellite scatterometer data [*Mears et al.*, 2001] who also attribute the discrepancy to the fact that, on average, the atmospheric boundary layer over the world ocean is slightly unstable. This bias is acceptably small. Even so, this paper focuses on wind speeds generally greater than 5 m/s in spring and summer. Higher wind speed induces neutrality in the atmospheric boundary layer [*Hsu et al.*, 1994]. The stability assumption seems especially plausible given the wind speeds considered and the lack of dramatic sea to air temperature differences in eastern ocean basins in spring and summer.

[24] QSCAT scatterometer wind estimates feature dense sampling within each swath. However, a sampling rate of just two swaths per day can lead to aliasing of measured winds for processes encompassing relatively small spatial and temporal scales [*Schlax et al.*, 2001]. Following *Schlax et al.* [2001], monthly means and composites constructed in this paper have sufficient temporal averaging such that sampling error will not be problematic. It should be noted that sampling error could be further reduced with more data and the QSCAT instrument is still functioning at the time of submission of this paper.

[25] The study region is along the western coast of North America extending offshore to 180° , and from 10 to 45°N (Figures 1 and 2). Backscatter from land received from antenna sidelobes contaminates wind estimates within 30 km of the coast. Satellite wind estimates immediately along the coast (within 30 km) are not a focus of this study and grids adjacent to the coast have been set to missing values. The QSCAT orbit provides twice-daily coverage. Ascending and

Table 2. QSCAT Satellite Orbit Pass Times

Range (Longitude)	UT	Orbit
115–140°W	1300–1400	ascending
140–155°W	1500	ascending
115–125°W	0100	descending
125–155°W	0200–0300	descending

descending swaths are separated by about 12 h. Each pass covers the study region in approximately 3 h (Table 2).

3. Methods

3.1. Wind Event Definition

[26] Wind events are defined by threshold exceedance for a given percentage of subsequent observations (Figure 3). The initiation of a wind event occurs when the projected buoy wind speed exceeds the 75th percentile of monthly mean wind speed for the initial hour and 18 of the subsequent 35 h. A new event cannot be defined until wind speed remains below the 75th percentile for 36 consecutive hours. Events are defined to capture the peaks evident in the time series while preventing overlapping events, and yet allowing for brief wind fluctuations (drops below the threshold wind speed evident in Figure 4). The events are identified using the time series of winds projected onto the dominant wind direction (DWD, the most common wind direction). Thus projected winds represent the component of wind speed along the DWD. The projected winds are used

to avoid contamination of the signal of interest by infrequent, but occasionally strong, southerly winds.

3.2. Wind Event Composites

[27] Wind events described above were used as the basis for composites. For each wind event, composites are made at not just the target time, but at 24 h intervals for 48 h before the event to 144 h after the start of the wind event. Thus lagged composites collectively reflect the mean evolution of the wind event.

3.3. Calculation of Anomalies

[28] Standardized anomalies are computed using a climatological mean and standard deviation obtained using data across all years. The climatological value is derived from a 30 d window surrounding the target day. The computation is done separately for each measurement of the day such that the process removes both seasonal and diurnal cycles.

4. Analysis

[29] Much of the temporal character of winds can be seen in a simple time series from coastal buoys (Figures 3 and 4) and noted in previous studies. Spring and summer have generally stronger wind with intermittent, short-duration drops in wind speed [Huyer, 1983; Beardsley *et al.*, 1987]. Peak northwest winds in spring usually last less than 5 d while wind events lasting 1–3 weeks or more tend to occur in late spring through summer [Caldwell and Stuart, 1986; Winant *et al.*, 1988].

[30] Winds are from the northwest, unless the wind is weak [Nelson, 1977; Dorman and Winant, 1995]. At B14,

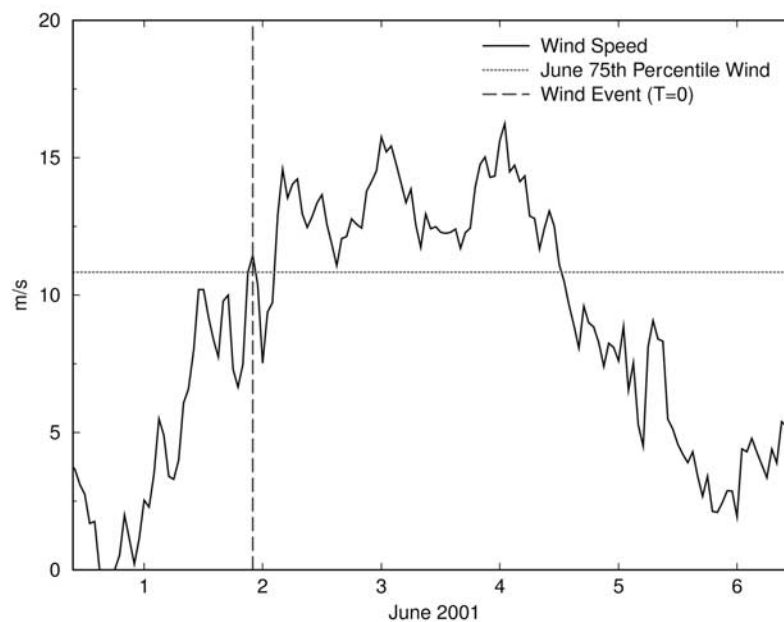


Figure 3. Wind event example. A wind event is identified in buoy wind at 2000 UT on 1 June 2001 (dashed vertical line). The horizontal line is the 75th percentile wind speed at buoy 46014 for the climatological (1981–2005) mean for the month of June. The dotted vertical line marks the initiation of the event, when the wind speed at the initial hour and 18 of the subsequent 35 h are above the 75th percentile. A new event cannot be defined until wind speed remains below the 75th percentile for 36 consecutive hours.

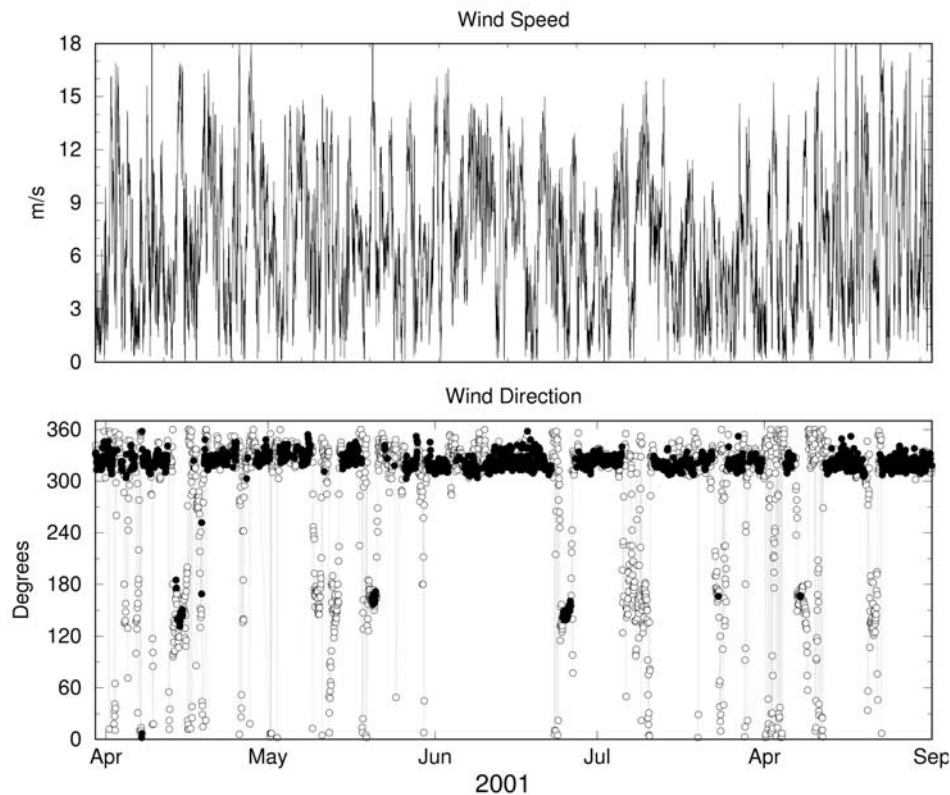


Figure 4. Hourly time series of wind speed and wind direction at Point Arena (B14) for 2001. Solid and open circles represent winds greater than 7.5 m/s and less than 7.5 m/s, respectively. Spring and summer winds are persistently from the northwest. Stronger winds seldom come from a direction other than the northwest.

for example, strong wind is aligned with the terrain, either from northwest or southeast with a tendency for light easterly winds (Figures 4 and 5a).

[31] The persistence in wind speed and direction in Figure 4 is representative of wind observed at other buoys along the coast (Figure 5) and other years (not shown). Winds seldom vary from this northwest to southeast orientation of the coastline (Figure 5a). Stronger winds are associated with persistent northwest wind direction. However, B59 experiences the most deviation from a pure, steady northwest direction seen at coastal buoys. Note that B59 is far offshore and in the storm track and thus experiences the least coastal influence and bears the brunt (and southerly wind) of winter cyclones.

[32] Figure 5b reveals interesting features of the seasonal cycle of projected winds. Projected winds refer to the component of wind in the direction of the dominant wind direction (DWD, the most common wind direction). There is a clear seasonal cycle with features that are common across all buoys. For the two coastal buoys (B14 and B63), highest wind speeds occur in spring when the entire wind distribution is shifted toward higher speed. Winds are seldom weak from early spring through summer (as opposed to late fall and winter when winds tend to be calm). However, moderate winds at all buoys are most consistent during August-September.

[33] From Figure 4 and previous research described in the background section, it is evident that persistent northwesterly winds in spring and summer are broken up by intermittent, short-duration calm periods. The temporal wind pattern can be thought of in terms of wind events. The literature roughly quantifies the duration of qualitatively defined wind events. Wind events last 1–2 d [Halliwell and Allen, 1987], 2–5 d [Caldwell and Stuart, 1986], and “several days” [Huyer, 1983; Winant et al., 1988; Beardsley et al., 1987]. Beardsley et al. [1987] describe northwesterly winds of 7–15 m/s lasting up to 30 d. However, they also highlight an enhanced northwesterly wind event lasting a week (1–7 June 1982) in the vicinity of Point Arena. Coastally trapped southerly surges are not considered here, but are discussed elsewhere [e.g., Mass and Bond, 1996; Nuss et al., 2000].

[34] The quantitative definition of wind events described in the Methods section will be useful for further analysis. Temporal wind events are based on percentile wind speed (Table 3) and specified duration in hourly observations at B14 for the April-August seasons from 1981 to 2005. Refer to the Methods sections for more details. The 75th percentile wind speed threshold was arbitrarily selected after considering the 85th and 65th percentiles. The statistics of events defined by all three (65th, 75th, and 85th percentile) thresholds are similar (Figure 6). The 75th percentile was chosen because the number, duration, and mean wind speed

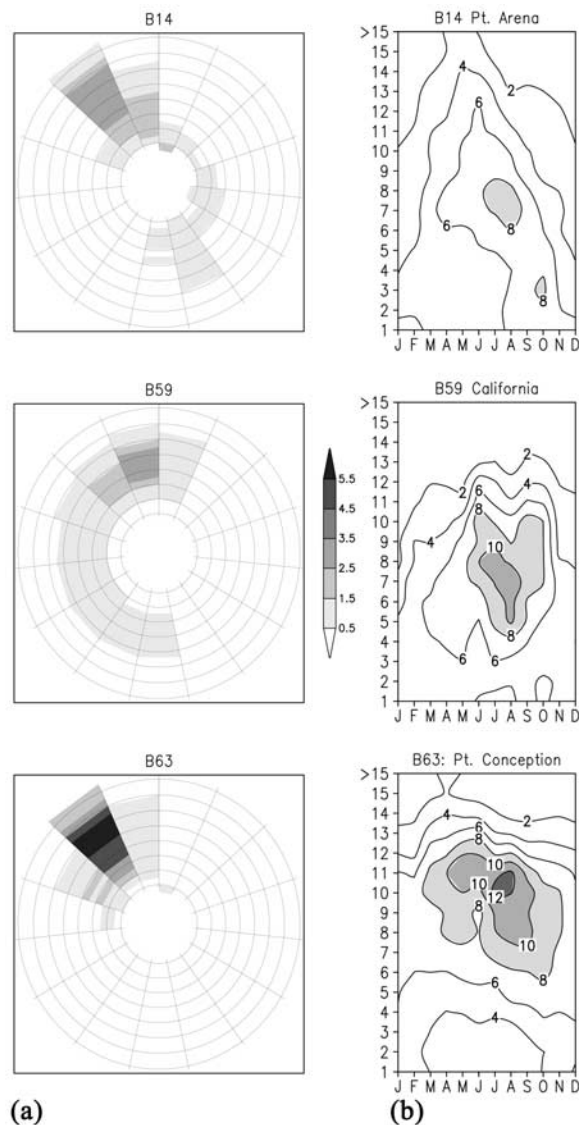


Figure 5. (a) Buoy wind roses calculated from long-term hourly buoy records in Table 1. Shading indicates percentage of observations within the specified speed-direction bin. Wind direction is indicated by compass reference (north is 0° , 360°) at 24° intervals. Wind speed is indicated by distance from the origin. Grid lines are spaced at 2 m/s intervals beginning with 2 m/s extending outward to 16 m/s. (b) Seasonal cycle of projected buoy winds. Projected winds refer to the component of wind in the direction of the dominant wind direction (DWD, the most common wind direction). Contours and shading indicate the percentage of projected observations at the specified speed and month.

of events seemed a better (subjective) fit. Under this definition, the frequency and duration of wind events is shown in Figure 6 for the Point Arena buoy (B14).

[35] Figure 6 shows that a substantial amount of time is occupied by wind events with duration greater than 5 d. Though synoptic events (1–5 d) are more frequent, events lasting longer than the synoptic timescale (>5 d) comprise more than 40% of total time within all wind events (Figure 6,

bottom). Note that, for the given event definition, it is impossible to have more than thirteen, 10-d events in the April–August season.

4.1. Coastal Wind Speed and Wind Stress Anomalies

[36] Lagged composites of the hourly buoy data from 1981 to 2005 are used to determine the average evolution of wind events during the April–August season. Composites are made at 24 h intervals from 48 h before to 144 h after the start of a wind event. Near Point Arena, wind stress anomalies measured at B14 are directed toward the north-northwest in the 2 d leading up to typical wind events (Figure 7). Anomalous speed and wind stress reverse direction, and turn toward the south-southeast and peak 24 h after the start of a wind event. Peak wind speed and along-coast wind stress anomalies reach roughly 1.5 standard deviations (Figure 7). Wind anomalies fall rapidly to near zero 96 h after the start of the wind event.

4.2. Atmospheric Circulation Associated With Wind Events

[37] The buoys have excellent temporal resolution (hourly) and sufficient record length (generally 10–20 years) for robust features. Collectively, the buoy measurements hint at spatial coherence (not shown). Fortunately, satellite wind measurements and NCEP global reanalysis fields are available to determine spatial structure.

[38] Upper air circulation features during wind events are characterized by an elevated ridge centered offshore near 135°W and 35°N , troughing along the coast, and relatively low 500 mbar heights over western North America (Figures 8a and 8b). The result is highly packed surface isobars along the California coast (Figure 8c) and a strengthened North Pacific surface high shifted eastward toward the coast. Figure 8d indicates the anomalous surface circulation involves both higher surface pressure offshore and lower surface pressure to the east over southwestern North America, suggesting wind events considered herein are a result of large-scale circulation features and dynamical influences, rather than localized thermal or topographical effects. Similar circulation features were described by *Winant et al.* [1988] for individual episodes of enhanced down coast surface wind.

4.3. Evolution of Wind Events

4.3.1. Evolution of Wind Event Composites of QSCAT Fields

[39] Scatterometer estimates reveal the spatial extent and persistence of intermittent northwesterly winds along the U.S. West Coast and eastern North Pacific Ocean. The buoy wind time series (Figure 4), show that intermittent brief periods of low wind are separated by typically much longer duration windy periods. QSCAT scatterometer data are available twice daily for (at least) the last 6 years with 25 km horizontal resolution and may be used to provide insight into the spatial structure of surface wind. The scatterometer data are used to examine spatial features of wind events determined from buoy time series. Wind events are defined as in Figure 3 and duration statistics shown in Figure 6. Initial wind event times (zero lag) are listed in Table 3. Composites from -24 h before to $+96$ h after initiation of wind events are examined.

Table 3. Wind Event Dates at Point Arena (B14)^a

Event Number	Year	Month	Day	Hour, UT
1	1999	Jul	2	0600
2	1999	Jul	8	0500
3	1999	Aug	5	0500
4	1999	Aug	14	1800
5	1999	Aug	21	0900
6	1999	Aug	31	0800
7	2000	May	17	1500
8	2000	May	25	0800
9	2000	May	29	2300
10	2000	Jun	23	0600
11	2000	Jul	3	0500
12	2000	Jul	26	0500
13	2000	Aug	14	0500
14	2001	Apr	10	1900
15	2001	Apr	22	0500
16	2001	May	2	0600
17	2001	May	10	0500
18	2001	May	17	2000
19	2001	May	29	2000
20	2001	Jun	2	2200
21	2001	Jun	13	2300
22	2001	Jul	1	0600
23	2001	Jul	15	0600
24	2001	Jul	29	0600
25	2001	Aug	16	0700
26	2001	Aug	26	0600
27	2002	Apr	15	1800
28	2002	Apr	19	1800
29	2002	Apr	26	2000
30	2002	May	6	0200
31	2002	May	14	2200
32	2002	May	31	0200
33	2002	Jun	20	0400
34	2002	Jul	4	1200
35	2002	Aug	7	0400
36	2002	Aug	19	0400
37	2002	Aug	26	1800
38	2003	Apr	18	1900
39	2003	May	8	1300
40	2003	May	15	1300
41	2003	Jun	16	0500
42	2003	Jun	22	1500
43	2004	Apr	9	0400
44	2004	May	10	1800
45	2004	May	30	0400
46	2004	Jun	12	0300
47	2004	Jun	15	0500
48	2004	Jun	28	0200
49	2005	Apr	10	0400
50	2005	Apr	15	0200
51	2005	Apr	18	1000
52	2005	May	23	1400
53	2005	Jun	1	0300
54	2005	Jun	12	0400
55	2005	Jul	3	0600
56	2005	Aug	30	1000

^aThe times noted are for start time (zero lag) hour of wind events identified in the buoy time series as in Figure 3 in section 3.1. The study period is April–August seasons from 2000 to 2005.

[40] The most notable feature of the composites is that their spatial extent and coherence is maintained for several days over a surprisingly large area (Figure 9). The pattern is consistent with the sea level pressure composite in Figure 8. *Schwing et al.* [2006] demonstrate that upwelling variations along the U.S. West Coast on seasonal timescales are associated largely with surface pressure anomalies over the eastern North Pacific. From inception to dissipation, events extend from northern California to include or con-

nect with the northeast trade wind region. At lag -24 h, winds are relatively weak along the coast (8 m/s extending 5° longitude from the southern California coast). Winds are below 8 m/s offshore several degrees from the coast heading southwest until they peak in the northeast trade wind region (around 10°N , 180° longitude). At lag $+24$ h, winds are greater than 10 m/s immediately at the coast from the California–Oregon border southward to Baja, Mexico, and extending out roughly 5° to the west. A region of winds at least 8 m/s continues to extend farther southwest from the coastal peak to connect and pick up with the northeast trades. The peak speeds of the northeast trades increase and extend farther northeast (Figure 9). After 4 d (lag $+96$), a signal is still evident, though wind speeds are universally weaker. Winds are generally weaker and less variable between the relatively strong winds along the California coast and the northeast trade wind region (800–2000 km southwest of California).

[41] In Figure 10, the spatial scale and magnitude of wind anomalies associated with strong wind close to the California coast at Cape Mendocino are revealed. The spatial coherence of wind events is more easily seen in composites of wind anomalies (Figure 10) than wind fields (Figure 9). At lag $+24$ h, winds are at least 0.8 standard deviations above normal in a region extending almost 15° longitude from the coast, and at least 0.4 standard deviations over a full 25° longitude (Figure 10).

4.3.2. Statistical Significance of Wind Event Composites of QSCAT Fields

[42] A Monte Carlo simulation was run to generate one hundred sets of simulated composites computed as in Figures 9 and 10 for times in Table 3. However, the year value in Table 3 was randomly switched before computing each of the 100 simulated composites, providing a benchmark of random simulated composites with identical statistical sampling (a type of bootstrapping statistical method). Each simulated composite element is constructed from the same number (56) of field maps with the same sequencing (lag -24 h, lag 0 h, lag $+24$ h, etc.) and similar annual and seasonal representation as the original composite in Figures 9 and 10. At each grid location, the original composite wind anomaly values are ranked relative to the simulated values. Positive wind anomaly data values in Figure 10 are plotted only if their rank is one (1st of 100) relative to the simulated values at a particular grid location (shading). Similarly, negative values are plotted only if their rank is 10 or below (labeled contours, no shading). Other grid values of the original composite (rank 11 to 99) are masked out in Figure 10. This Monte Carlo analysis of uncertainty suggests the spatial structures in Figure 10 are unlikely to arise by chance.

[43] Another buoy located south of Point Arena was used to explore the robustness of the composite pattern seen in Figures 9 and 10 based on B14 at Point Arena. The Point Conception Buoy, 46063 (B63: 34.25°N , 120.66°W), is located near Point Conception and 600 km south-southwest of B14 (39.22°N , 123.97°W). Wind speeds (not shown) are slightly and universally greater at all composite times for wind field composites based on Point Conception (B63), relative to Point Arena (B14). Wind events identified at B63 are mostly unique. Only 15% of wind events identified at buoy 14 match (within 24 h) events at B63. Even so, the

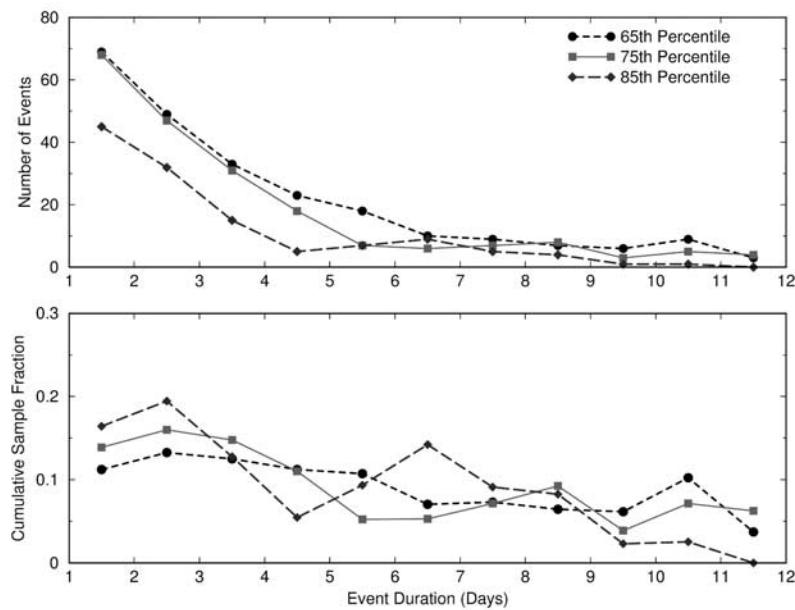


Figure 6. Wind event frequency-duration threshold. The x axis is duration of individual wind events defined in the text and in Figure 3. (top) The y axis is the number of events identified (of a given duration and exceeding indicated frequency) during April–August of 1981–2005 for buoy 46014. Threshold wind speeds of 65th, 75th, and 85th percentile wind speed for all events considered were used in the event definition to test the stability of event frequency. Only the 75th percentile is used in subsequent analyses. (bottom) The sample fraction of cumulative event duration is the combined time among all counted events, of a given duration, divided by the total combined duration of all events.

composite patterns of standardized wind speed anomalies for both buoys are similar for all composite times. The magnitude and spatial pattern of wind speed composites for B63 support the robustness of the wind event patterns.

4.3.3. Evolution of Wind Event Composites of QSCAT Fields for Select Locations

[44] The time series bring out what may be evident in the composite maps of wind speed anomaly; wind anomalies persist offshore from the coast longer than they do immediately along the coast. Figures 9e and 9f show stronger signals over the middle of the North Pacific Ocean than closer to the U.S. West Coast. Buoy winds and wind stress anomaly components measured on B14 peak at lag = +24 h. Likewise, in Figure 11, wind speed and wind stress anomaly components from QSCAT fields for location 1 (124.75°W, 37.0°N; Figure 12 maps locations 1–4 in Figure 11) and location 2 (128.0°W, 27.75°N) also peak at lag = +24 h. However, peak wind speed anomalies occur at lag +48 h at location 3 (141.0°W, 26.0°N, Figure 11a). At lag = +72 h, along-coast wind stress anomalies reach their peak for location 3 (Figure 11b), while wind speed anomalies remain relatively strong at lag +96 h for locations 3 and 4 (Figures 11a–11c). Another difference between the coastal region and farther offshore region is that the across-coast component of wind stress switches sign. The buoy indicates positive across-coast wind stress anomaly (directed onshore) while the across-coast wind stress is directed offshore for all locations in Figure 12.

4.3.4. Wind Events and Ocean Circulation Anomalies

[45] Anomalous northerly winds during wind events drive anomalous ocean circulation. Figure 13 shows the anoma-

lous wind stress and resulting anomalous Ekman transport. Anomalous Ekman transport is directed toward the center of the eastern North Pacific Ocean (roughly 30°N, 135°W). Also evident is relatively strong Ekman transport anomaly directed away from the U.S. West Coast. The resulting

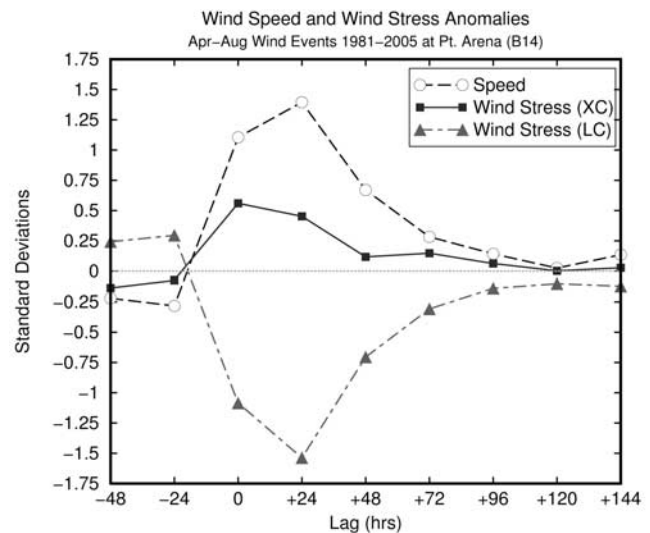


Figure 7. Coastal wind speed and wind stress anomalies at buoy 14. Wind stress is expressed in terms of across-coast (XC) and along-coast (LC) components. South of Cape Mendocino (including the location of B14) the coastal orientation is 28° east of due south.

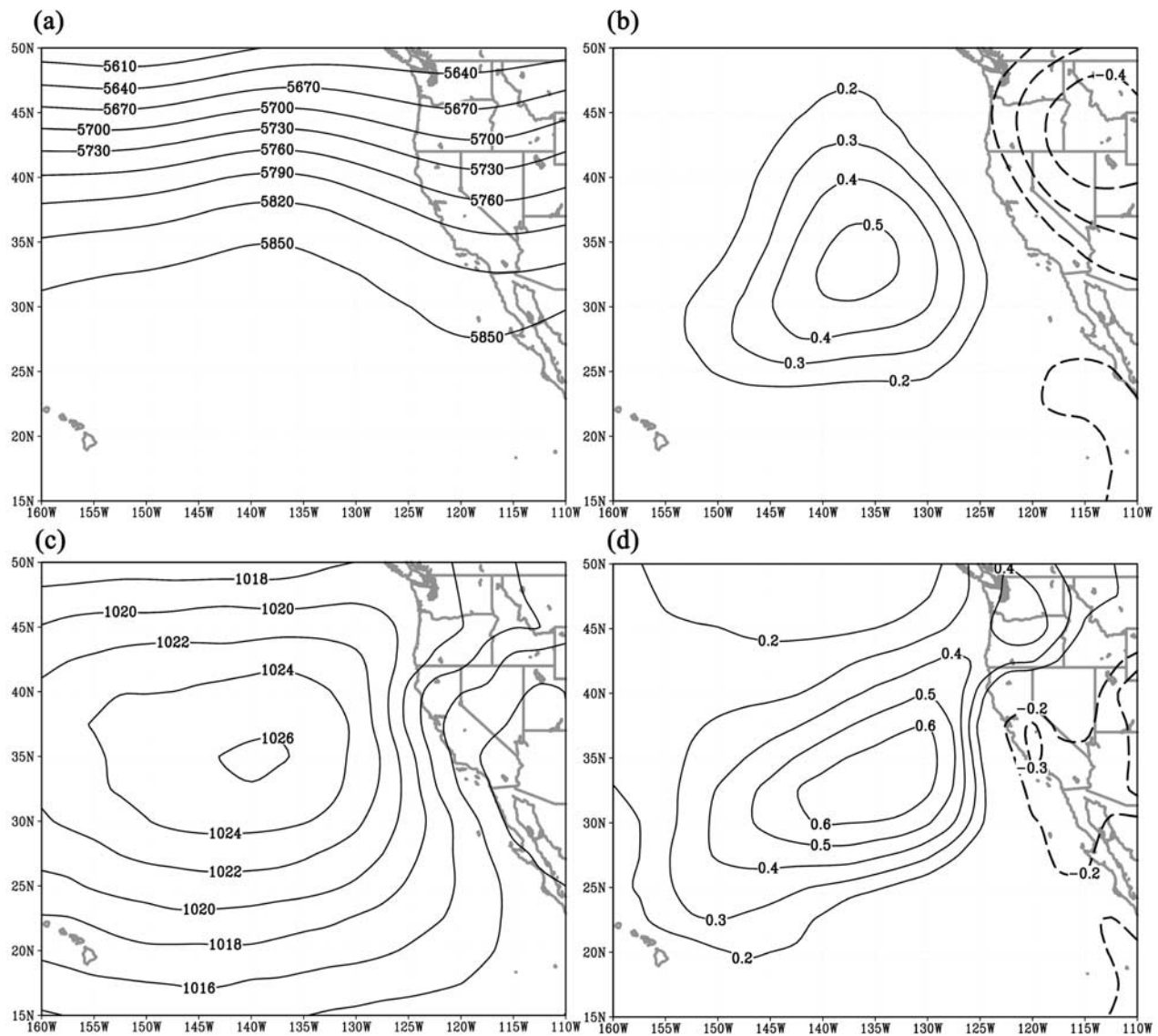


Figure 8. SLP and 500 mbar height circulation associated with wind events. The images depict the fields for lag +48 h. (a) The 500 mbar heights in meters. (b) The 500 mbar height anomalies in standard deviations. (c) Sea level pressure in millibars. (d) Sea level pressure anomaly in standard deviations.

convergence of mass in the eastern North Pacific Ocean implies enhanced sea surface height and gyre circulation. Anomalous Ekman transport away from coast as indicated in Figure 13 for lag +24 h may drive enhanced coastal upwelling and/or more vigorous along-coast currents.

[46] A clearer picture of the upwelling and downwelling patterns can be seen in Figure 14, which depicts the curl of wind stress anomalies. The curl of wind stress anomaly, $\nabla \times \vec{\tau}$, reflects upwelling in the wind driven layer. The curl of wind stress is the same as the divergence of Ekman transport. Anomalous convergence of Ekman transport indicates downwelling (negative wind stress curl anomaly), while divergence indicates upwelling (positive wind stress curl anomaly). Note, however, that derivative fields are notoriously noisy over relatively small spatial scales. Only persistent large-scale features are discussed below.

[47] Wind events substantially affect not just the coastal region, but also coherently affect Ekman pumping one

thousand km or more offshore from the coast. Just before the wind event, there is downwelling along the central and southern California coasts (Figure 14a). Offshore of the southern California and northern Baja coasts, the sign switches and upwelling can be seen 24 h later when the wind event starts (Figure 14b). Farther offshore, there are hints of a broad region dominated by weak downwelling anomalies at zero lag.

[48] Weak anomalies far offshore become strong by lag +24 h (Figure 14c), when a relatively robust and widespread downwelling anomaly pattern can be seen extending from Cape Mendocino southwest to 135°W, 30°N. Downwelling can also be seen along the coast from Canada southward to Point Arena. At the same time, the region of strong upwelling anomaly offshore of southern California and northern Baja expands and strengthens.

[49] The patterns seen at lag +24 h persist and are similar at lag +48 h, but with weaker downwelling far offshore and

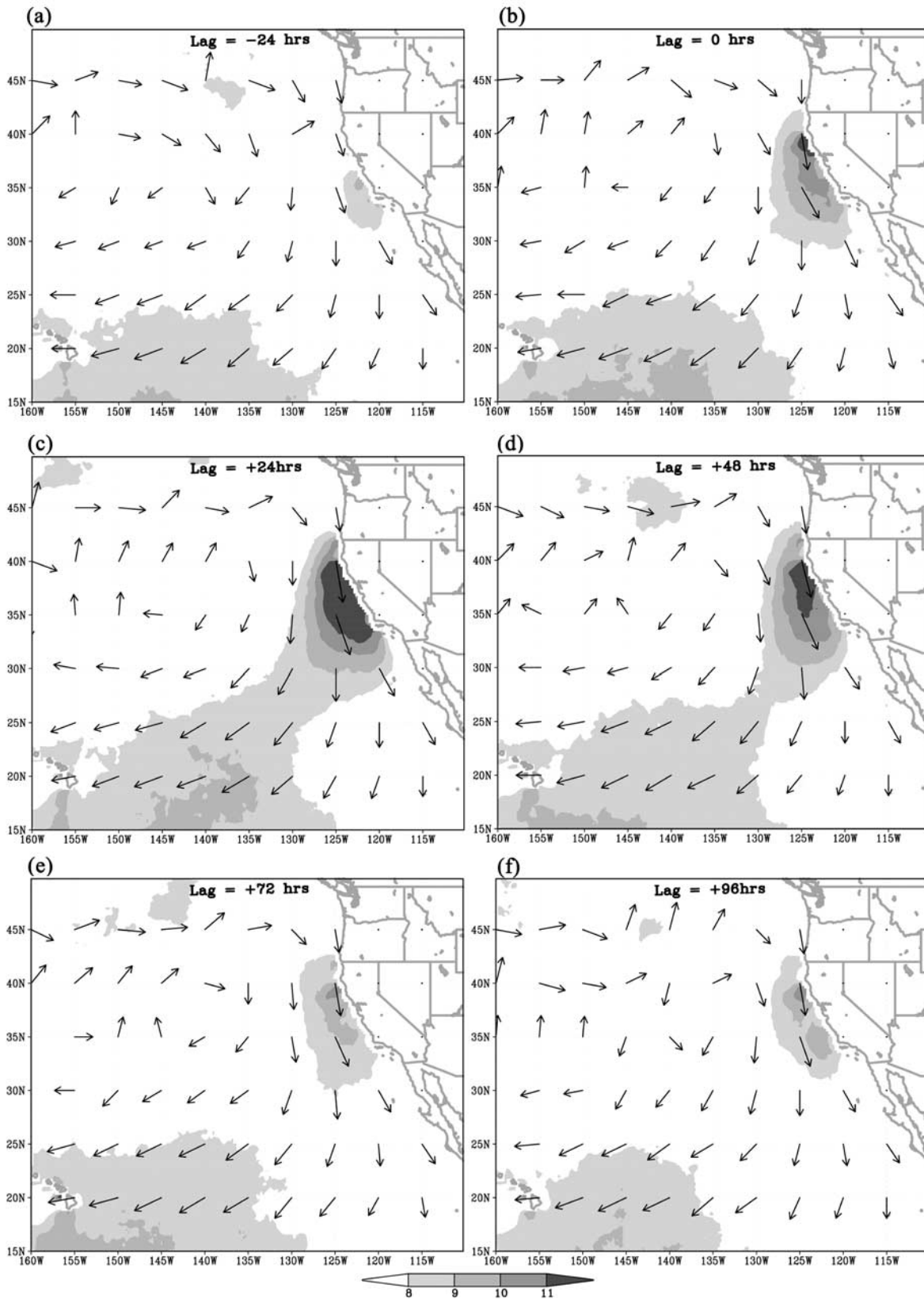


Figure 9. Composite evolution QSCAT wind field for wind events in Table 3. Wind speeds are in m/s. Arrows indicate the dominant wind direction in each composite map and are plotted at every 20th grid point. The composite maps are shown at intervals relative to zero lag as defined in Figure 3.

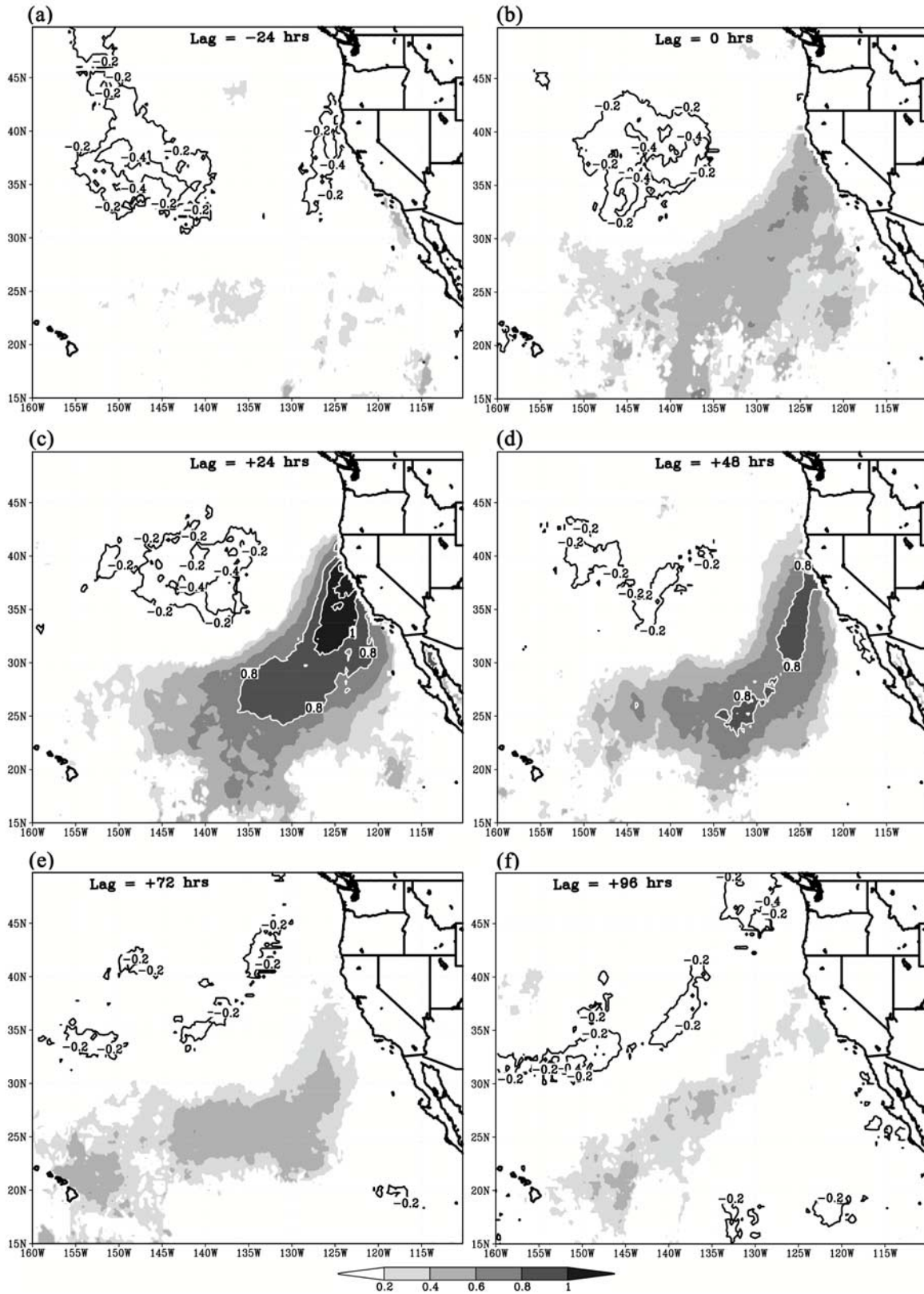


Figure 10. Evolution of composites of QSCAT wind anomalies for wind events in Table 3. The contours and shading are in units of standard deviations. Shaded areas include only those positive grid values ranked 1st relative to 100 random composites from a Monte Carlo simulation. Negative contours are plotted only when the values rank in the bottom 10/100.

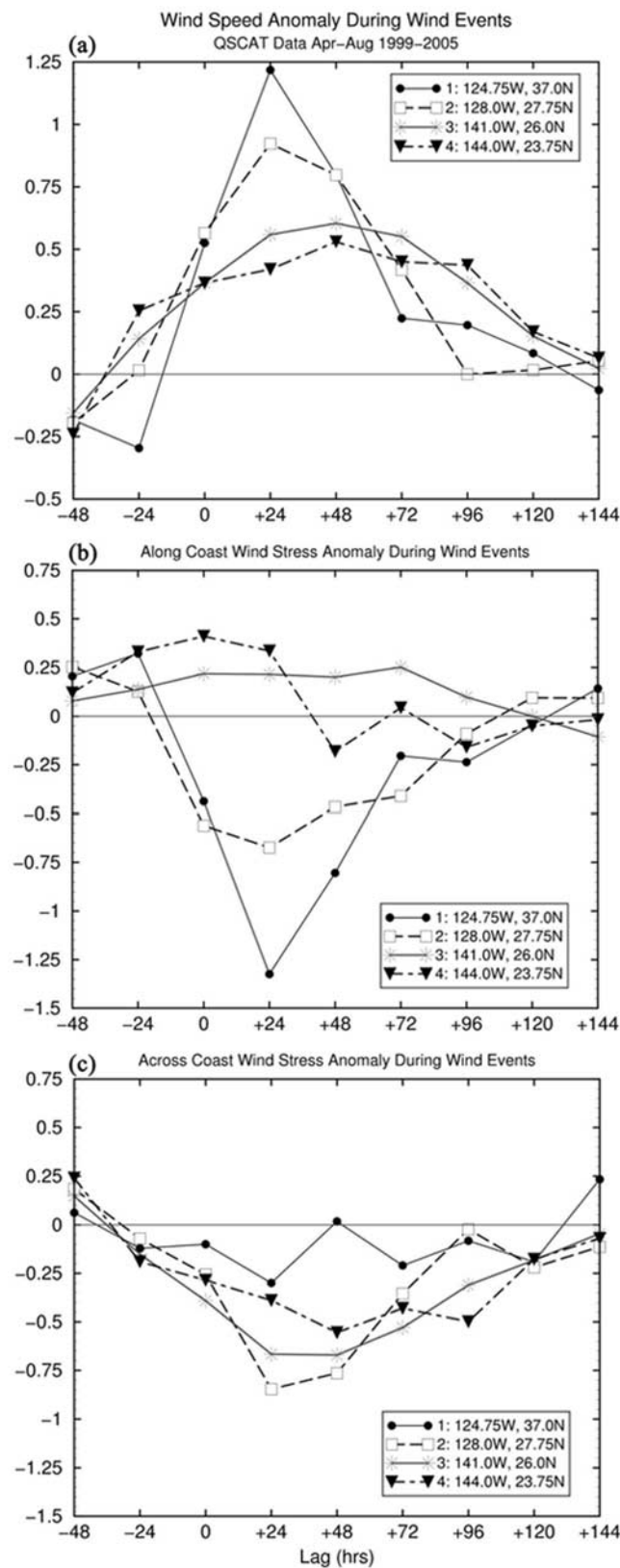


Figure 11. Evolution of anomalies in units of standard deviations for various points over the North Pacific (from QSCAT data). Locations are indicated in Figure 12. (a) Wind speed, (b) along-coast wind stress, and (c) across-coast wind stress.

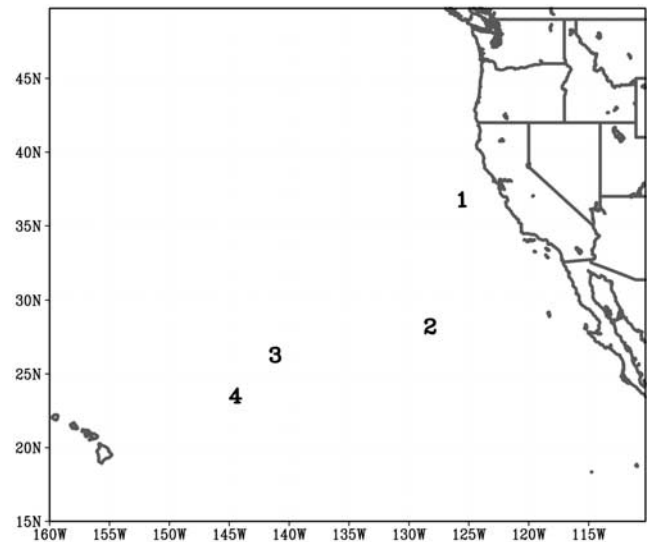


Figure 12. Map indicating locations 1–4 described in Figure 11. South of Cape Mendocino (including all locations plotted here) the coastal orientation is aligned northwest to southeast, 28° from due south.

stronger upwelling along the central California coast. A couplet of upwelling and downwelling is aligned southwest to northeast extending southwestward beginning near the entrance to the San Francisco bay.

5. Concluding Remarks

[50] Persistent spring and summer northerly surface winds are the defining climatological feature of the west coast of North America, especially from Cape Mendocino southward, and are important for upwelling and a vast array of other biological, oceanic, and atmospheric processes.

[51] This paper seeks to quantify the intermittence of northerly coastal winds, define wind events, and examine some consequences of typical wind events. Temporal statistics of wind events using different wind speed thresholds at buoy 14 near Point Arena were made and a subjective choice of 75th percentile threshold wind speed was used for further analysis. Peak northwesterly winds in spring and summer usually last 1–3 d with frequency 1–4 events per month and cover a spatial scale of several degrees in both longitude and latitude. Events lasting over 1 week can occur. About 40% of the combined event time is occupied by events lasting longer than the synoptic timescale (1–5 d).

[52] To examine the spatial structure and evolution of wind events, composites were created of buoy wind speed, atmospheric circulation from NCEP global reanalysis fields, and surface wind estimates from QSCAT satellite scatterometer data based on the wind event definition.

[53] QSCAT satellite scatterometer wind measurements combined with a quantitative definition of wind events allowed examination of the variability and evolution of wind over the eastern North Pacific Ocean with unprecedented detail. The spatial extent, temporal variability, and space-time coherence of wind events over several days

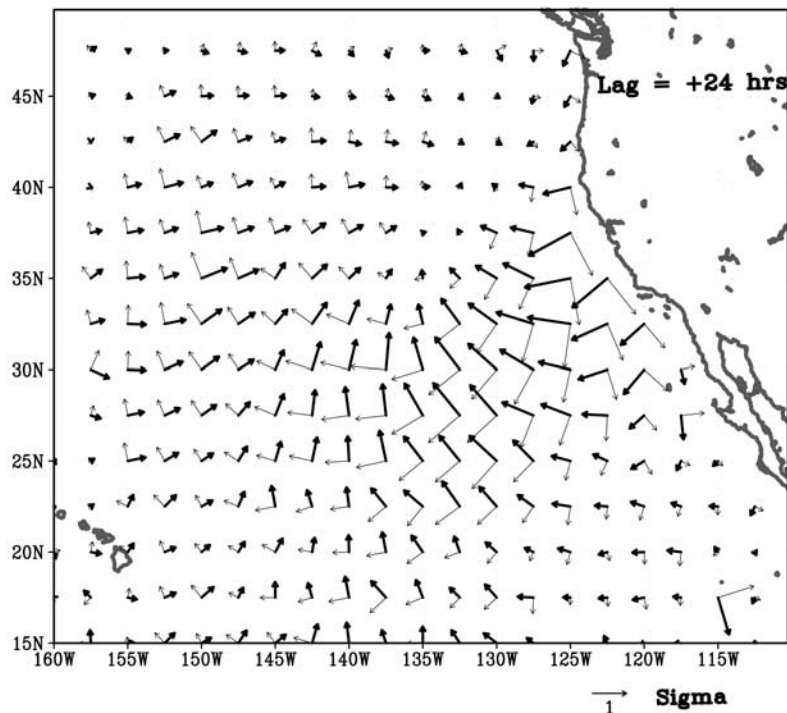


Figure 13. Ekman transport anomaly (in bold) and wind stress anomaly vectors at lag +24 h. Data are for wind events in Table 3 and derived from QSCAT composites of fields (1999–2005). Units are standard deviations and vectors are plotted at every 10th grid point.

could not be determined from spatially limited station observations, monthly means from satellite or ship reports, or intensive observation campaigns.

[54] Because the offshore region has suffered particular neglect because of lack of data farther offshore, details of large-scale wind events quantified in this paper are an interesting supplement and contrast to observational studies of wind along the U.S. West Coast and the relatively smooth offshore winds in model generated fields.

[55] Composites of QSCAT scatterometer wind fields were created from 56 wind events based on percentile wind speed from an offshore buoy for the April–August seasons for the time period of 20 July 1999 to 31 August 2005. The composite maps of wind speed anomaly highlight large and regional-scale surface wind anomaly pattern over the eastern North Pacific Ocean that grows broad and spreads over the southern portion of the eastern North Pacific Ocean extending into the northeast trade wind portion of the subtropical high-pressure system.

[56] Spatially and temporally coherent events lasting days are driven by large-scale forcing from interaction between the thermal low over the southwestern United States and the eastern North Pacific high-pressure system. This notion is supported by SLP composite maps (Figure 8), which indicate that wind events are part of a large-scale atmospheric circulation. The spatial pattern of wind events is more robust in composites of QSCAT surface wind anomalies and surprisingly different from the high-wind regions seen in the composite of QSCAT wind fields.

[57] Winds offshore measured from QSCAT satellite persist longer than the wind measured at the coastal buoy

during a typical wind event. The coastal winds peak sharply and typically last 72 h. Farther offshore, winds peak more slowly and typically last 96 h.

[58] The evolution of surface wind anomalies during wind events drives anomalous ocean circulation features that extend over 1000 km offshore from the west coast of North America. Anomalous wind stress during wind events fuels anomalous Ekman transport divergence along the immediate coast, and convergence farther offshore, near 135°W, 30°N. Along the immediate coast and south-southwest of southern California, strong downwelling anomaly preceding wind events switches to a strong upwelling anomaly for the subsequent 48–72 h. The upwelling features are not tied to the coast but extend over 500 km southwest of the southern California coast. The coastal upwelling anomaly feature also extends northward toward the San Francisco Bay entrance and offshore 200–300 km from the central California coast. The upwelling anomaly offshore of central California peaks 48 h after the start of a wind event.

[59] A broad downwelling anomaly feature extends from Cape Mendocino southwest to 140°W, 35°N. The feature covers over 1000 km in both latitudinal and meridional directions. The downwelling anomaly feature also persists for at least 72 h.

[60] Though a comprehensive discussion of the implication of these upwelling patterns for other features of ocean circulation dynamics and for ecosystems in the California current and the eastern North Pacific Ocean are beyond the scope of this paper, these topics are significantly interesting to merit further consideration.

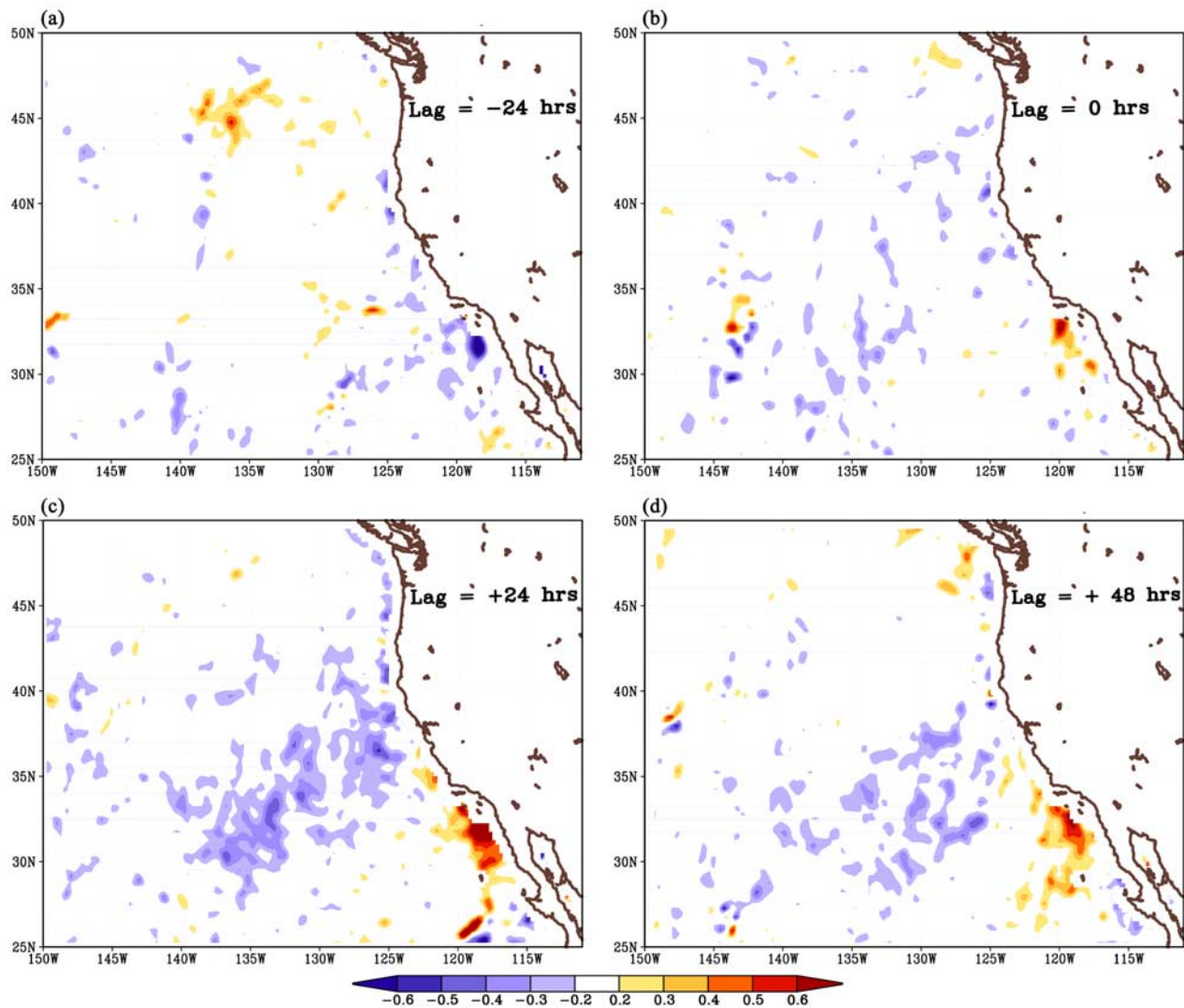


Figure 14. Curl of wind stress anomaly for (a) lag -24 h, (b) zero lag, (c) lag $+24$ h, and (d) lag $+48$ h. Data are for wind events in Table 3 and derived from QSCAT composites of fields (1999–2005). Units are standard deviations. A nine-point spatial smoothing has been applied.

[61] The strength and variability of the offshore Ekman pumping may be of even more significant than previously believed. Hickey *et al.* [2006] suggest the California Current system may be forced by remote wind stress in addition to local wind forcing. Huyer [1983] indicates the importance of upwelling farther offshore for the California Current system. With the prospect of climate change and its effects on the California Current Ecosystem [Bakun, 1990; Synder *et al.*, 2003; Grantham *et al.*, 2004; Pierce *et al.*, 2006], there is increased urgency in documenting and understanding offshore wind and Ekman pumping features.

[62] Additional studies may also focus on implications of the strength, duration, and spatial extent of wind events for the structure and variability of moisture and temperature in the marine boundary layer, distribution of aerosols, strength and variability of offshore oceanic upwelling, oceanic circulation, and the sea state. Such studies could benefit from the continuing archive of QSCAT satellite data (the instrument is still in operation at the time of submission of

this paper) and blended products for information between swaths and closer to the coast [e.g., Chao *et al.*, 2003].

[63] **Acknowledgments.** This research was supported by a student assistantship to the first author by the Board of Directors of the Hydrologic Research Center, a public benefit corporation. Additional support was provided by Scripps Institution of Oceanography at the University of California, San Diego, through the California Applications Project. The California Applications Project is sponsored by the National Oceanic and Atmospheric Administration. We would also like to express our gratitude to three anonymous reviewers whose comments proved very useful in shaping the direction of this paper and some of its more interesting results.

References

- Bakun, A. (1990), Global climate change and intensification of coastal ocean upwelling, *Science*, *247*, 198–201.
- Bakun, A., and C. S. Nelson (1991), Wind stress curl in subtropical eastern boundary current regions, *J. Phys. Oceanogr.*, *21*, 1815–1834.
- Baynton, H. W., J. M. Bidwell, and D. W. Beran (1965), The association of the low-level inversions with surface wind and temperature at Point Arguello, *J. Appl. Meteorol.*, *4*, 509–516.

- Beardsley, R. C., C. E. Dorman, C. A. Friehe, L. K. Rosenfeld, and C. D. Winant (1987), Local atmospheric forcing during the Coastal Ocean Dynamics Experiment: 1. A description of the marine boundary layer and atmospheric conditions over a Northern California upwelling region, *J. Geophys. Res.*, *92*(C2), 1467–1488.
- Bourassa, M. A., D. M. Legler, and S. R. Smith (2003), SeaWinds validation with research vessels, *J. Geophys. Res.*, *108*(C2), 3019, doi:10.1029/2001JC001028.
- Brost, R. A., D. H. Lenschow, and J. C. Wyngaard (1982), Marine stratocumulus layers: Mean conditions, *J. Atmos. Sci.*, *39*, 800–817.
- Burk, S. D., and W. T. Thompson (1996), The summertime low-level jet and MBL structure along the California coast, *Mon. Weather Rev.*, *124*, 668–686.
- Caldwell, P. C., and D. W. Stuart (1986), Mesoscale wind variability near Point Conception, California during spring 1983, *J. Clim. Appl. Meteorol.*, *25*, 1241–1254.
- Chao, Y., Z. Li, J. C. Kindle, J. D. Paduan, and F. P. Chavez (2003), A high-resolution surface vector wind product for coastal oceans: Blending satellite scatterometer measurements with regional mesoscale atmospheric model simulations, *Geophys. Res. Lett.*, *30*(1), 1013, doi:10.1029/2002GL015729.
- Chelton, D. B., and M. H. Freilich (2005), Scatterometer-based assessment of 10-m wind analyses from the operational ECMWF and NCEP numerical weather prediction models, *Mon. Weather Rev.*, *133*, 409–429.
- Chelton, D. B., M. G. Schlax, M. H. Freilich, and R. F. Milliff (2004), Satellite radar measurements reveal short-scale features in the wind stress field over the world ocean, *Science*, *303*, 978–983.
- Dabberdt, W. F., and W. Viezee (1987), South Central Coast Cooperative Aerometric Monitoring Program (SCCCAMP), *Bull. Am. Meteorol. Soc.*, *68*, 1098–1110.
- Dorman, C. E., and C. D. Winant (1995), Buoy observations of the atmosphere along the west coast of the United States, 1981–1990, *J. Geophys. Res.*, *100*(C8), 16,029–16,044.
- Dorman, C. E., and C. D. Winant (2000), The structure and variability of the marine atmosphere around the Santa Barbara Channel, *Mon. Weather Rev.*, *128*, 261–282.
- Dorman, C. E., D. P. Rogers, W. Nuss, and W. T. Thompson (1999), Adjustment of the summer marine boundary layer around Point Sur, California, *Mon. Weather Rev.*, *127*, 2143–2159.
- Dorman, C. E., T. Holt, D. P. Rogers, and K. A. Edwards (2000), Large-scale structure of the June–July 1996 marine boundary layer along California and Oregon, *Mon. Weather Rev.*, *128*, 1632–1652.
- Draper, D. W., and D. G. Long (2002), An assessment of SeaWinds on QuikSCAT wind retrieval, *J. Geophys. Res.*, *107*(C12), 3212, doi:10.1029/2002JC001330.
- Ebuchi, N., H. C. Graber, and M. J. Caruso (2002), Evaluation of wind vectors observed by QuikSCAT/SeaWinds using ocean buoy data, *J. Atmos. Oceanic Technol.*, *19*, 2049–2062.
- Edwards, K. A., D. P. Rogers, and C. E. Dorman (2002), Adjustment of the marine atmospheric boundary layer to the large-scale bend in the California coast, *J. Geophys. Res.*, *107*(C12), 3213, doi:10.1029/2001JC000807.
- Elliot, D. L., and J. J. O'Brien (1977), Observational studies of the marine boundary layer over and upwelling region, *Mon. Weather Rev.*, *105*, 86–98.
- Filonczuk, M. K., D. R. Cayan, and L. G. Riddle (1995), Variability of marine fog along the California coast, *Ref. 95-2*, pp. 102 pp., Scripps Inst. of Oceanogr., La Jolla, Calif.
- Fosberg, M. A., and M. J. Schroeder (1966), Marine air penetration in central California, *J. Appl. Meteorol.*, *5*, 573–589.
- Freilich, M. H., D. G. Long, and M. W. Spencer (1994), SeaWinds: A scanning scatterometer for ADEOS II—Science overview, *IGARSS '94 Int. Geosci. Remote Sens. Symp.*, *2*, 960–963.
- Gilhouse, D. B. (1987), A field evaluation of NDBC moored buoy winds, *J. Atmos. Oceanic Technol.*, *4*, 94–104.
- Grantham, B. A., F. Chan, K. J. Nielsen, D. S. Fox, J. A. Barth, A. Huyer, J. Lubchenco, and B. A. Menge (2004), Upwelling-driven nearshore hypoxia signals ecosystem and oceanographic changes in the northeast Pacific, *Nature*, *429*, 749–754.
- Haack, T., and S. D. Burk (2001), Summertime marine refractivity conditions along coastal California, *J. Appl. Meteorol.*, *40*, 673–687.
- Halliwell, G. R., and J. S. Allen (1987), The large-scale coastal wind field along the west coast of North America, 1981–1982, *J. Geophys. Res.*, *92*(C2), 1861–1884.
- Hamilton, G. D. (1980), NOAA Data Buoy Office programs, *Bull. Am. Meteorol. Soc.*, *61*, 1012–1017.
- Hickey, B., A. MacFadyen, W. Cochlan, R. Kudela, K. Bruland, and C. Trick (2006), Evolution of chemical, biological, and physical water properties in the northern California Current in 2005: Remote or local wind forcing?, *Geophys. Res. Lett.*, *33*, L22S02, doi:10.1029/2006GL026782.
- Hoskins, B. J. (1996), On the existence and strength of the summer subtropical anticyclones, *Bull. Am. Meteorol. Soc.*, *77*, 1287–1292.
- Hsu, S. A., E. A. Meindl, and D. B. Gilhouse (1994), Determining the power-law wind-profile exponent under near-neutral stability conditions at sea, *J. Appl. Meteorol.*, *33*(6), 757–765.
- Huyer, A. (1983), Coastal upwelling in the California Current system, *Prog. Oceanogr.*, *12*, 259–284.
- Kalnay, E., et al. (1996), The NCEP/NCAR 40-year reanalysis project, *Bull. Am. Meteorol. Soc.*, *77*(3), 437–471.
- Kanamitsu, M. (1989), Description of the NMC global data assimilation and forecast system, *Weather Forecasting*, *4*, 335–342.
- Kistler, R., et al. (2001), The NCAR-NCEP 50-year reanalysis: Monthly means CD-ROM and documentation, *Bull. Am. Meteorol. Soc.*, *82*, 247–267.
- Klein, S. A., D. L. Hartmann, and J. R. Norris (1995), Relationships among low cloud structure, sea surface temperature, and atmospheric circulation, *J. Clim.*, *8*, 1140–1155.
- Koracin, D., J. Lewis, W. T. Thompson, C. E. Dorman, and J. A. Businger (2001), Transition of stratus into fog along the California Coast: Observation and modeling, *J. Atmos. Sci.*, *48*, 1712–1721.
- Large, W. G., and S. Pond (1982), Sensible and latent heat flux measurements over the ocean, *J. Phys. Oceanogr.*, *12*, 464–482.
- Liu, W. T. (2002), Progress in scatterometer application, *J. Oceanogr.*, *58*, 121–136.
- Liu, W. T., and W. Tang (1996), Equivalent neutral wind, *JPL Publ. 96-17*, 8 pp., NASA Jet Propul. Lab., Pasadena, Calif.
- Liu, W. T., and X. Xie (2001), Improvement in spacebased scatterometers and increased scientific impact in the past decade, paper presented at Oceans 2001, Mar. Technol. Soc., Honolulu, Hawaii.
- Lorenz, E. N. (1969), The nature of the global circulation of the atmosphere: A present view, in *The Global Circulation of the Atmosphere*, pp. 3–23, R. Meteorol. Soc., London.
- Lovegrove, J. (2003), Redefining small craft advisory for hazardous seas, *Tech. Attach. 03-11*, 9 pp., Natl. Weather Serv., Western Reg., Salt Lake City, Utah.
- Mass, C. F., and N. A. Bond (1996), Coastally trapped wind reversals along the United States West Coast during the warm season, Part II: Synoptic evolution, *Mon. Weather Rev.*, *124*, 446–461.
- Mass, C. F., M. D. Albright, and D. J. Brees (1986), The onshore surge of marine air into the Pacific Northwest: A coastal region of complex terrain, *Mon. Weather Rev.*, *114*, 2602–2627.
- Mears, C. A., D. K. Smith, and F. J. Wentz (2001), Comparison of Special Sensor Microwave Imager and buoy-measured wind speeds from 1987 to 1997, *J. Geophys. Res.*, *106*, 11,719–11,729.
- Miller, A. J., et al. (1999), Observing and modeling the California Current System, *Eos Trans. AGU*, *80*, 533–539.
- Miyasaka, T., and H. Nakamura (2005), Structure and formation mechanisms of the Northern Hemisphere summertime subtropical highs, *J. Clim.*, *18*, 5046–5065.
- Münchow, A. (2000), Wind stress curl forcing of the coastal ocean near Point Conception, California, *J. Phys. Oceanogr.*, *30*, 1265–1280.
- Naderi, F. M., M. H. Freilich, and D. G. Long (1991), Spaceborne radar measurement of wind velocity over the ocean—An overview of the NSCAT scatterometer system, *Proc. IEEE*, *97*, 850–866.
- National Meteorological Center Development Division Staff (1988), Research version of the medium range forecast model, *NMC Doc. Ser. 1*, Washington, D. C.
- Neiburger, M., D. S. Johnson, and C.-W. Chien (1961), *Studies of the Structure of the Atmosphere Over the Eastern Pacific Ocean in Summer*, Univ. of Calif. Publ. in Meteorol., vol. 1, 58 pp., Univ. of Calif. Press, Berkeley.
- Nelson, C. S. (1977), Wind stress and wind stress curl over the California current, *NOAA Tech. Rep., NMFS SSRF-714*, 87 pp.
- Nuss, W. A., et al. (2000), Coastally trapped wind reversals: Progress toward understanding, *Bull. Am. Meteorol. Soc.*, *81*, 719–743.
- Parrish, R. H., F. B. Schwing, and R. Mendelsohn (2000), Midlatitude wind stress: The energy source for climatic regimes in the North Pacific Ocean, *Fish. Oceanogr.*, *9*, 224–238.
- Perlin, N., R. M. Samelson, and D. B. Chelton (2004), Scatterometer and model wind and wind stress in the Oregon–northern California coastal zone, *Mon. Weather Rev.*, *132*, 2110–2129.
- Pierce, S. D., J. A. Barth, R. E. Thomas, and G. W. Fleischer (2006), Anomalously warm July 2005 in the northern California Current: Historical context and the significance of cumulative wind stress, *Geophys. Res. Lett.*, *33*, L22S04, doi:10.1029/2006GL027149.
- Pincus, R., M. B. Baker, and C. S. Bretherton (1997), What controls stratocumulus radiative properties? Lagrangian observations of cloud evolution, *J. Atmos. Sci.*, *54*, 2215–2236.
- Rogers, D. P., et al. (1998), Highlights of coastal waves 1996, *Bull. Am. Meteorol. Soc.*, *79*, 1307–1326.
- Schlax, M. G., D. B. Chelton, and M. F. Freilich (2001), Sampling errors in wind fields constructed from single and tandem scatterometer datasets, *J. Atmos. Oceanic Technol.*, *18*, 1014–1036.

- Schwing, F. B., N. A. Bond, S. J. Bograd, T. Mitchell, M. A. Alexander, and N. Mantua (2005), Delayed coastal upwelling along the U. S. West Coast in 2005: A historical perspective, *Geophys. Res. Lett.*, *33*, L22S01, doi:10.1029/2006GL026911.
- Seager, R., R. Murtugudde, N. Naik, A. Clement, N. Gordon, and J. Miller (2003), Air-sea interaction and the seasonal cycle of the subtropical anticyclones, *J. Clim.*, *16*, 1948–1966.
- Snyder, M. A., L. C. Sloan, N. S. Diffenbaugh, and J. L. Bell (2003), Future climate change and upwelling in the California Current, *Geophys. Res. Lett.*, *30*(15), 1823, doi:10.1029/2003GL017647.
- Thompson, W. T., S. D. Burk, and J. Lewis (2005), Fog and low clouds in a coastally trapped disturbance, *J. Geophys. Res.*, *110*, D18213, doi:10.1029/2004JD005522.
- Wentz, F. J. (1997), A well-calibrated ocean algorithm for special sensor microwave/imager, *J. Geophys. Res.*, *102*(C4), 8703–8718.
- Winant, C. D., and C. E. Dorman (1997), Seasonal patterns of surface wind stress and heat flux over the Southern California Bight, *J. Geophys. Res.*, *102*, 5641–5653.
- Winant, C. D., C. E. Dorman, C. A. Friehe, and R. C. Beardsley (1988), The marine layer off Northern California: An example of supercritical channel flow, *J. Atmos. Sci.*, *45*, 3588–3605.
- Yen-Nakafuji, D. (2005), California wind resources, *CEC Publ. CEC-500-2005-071-D*, 31 pp., Calif. Energy Comm., Sacramento, Calif.

D. R. Cayan, K. P. Georgakakos, N. E. Graham, and S. V. Taylor, Scripps Institution of Oceanography, University of California, San Diego, La Jolla, CA 92093, USA. (staylor@hrc-lab.org)